AD-A182 913 AN EXPERIMENTAL STUDY OF SURFACE ROUGHNESS EFFECTS ON TURBULENT BOUNDARY..(U) MISSISSIPPI STATE UNIV MISSISSIPPI STATE DEPT OF MECHANICAL A.. 1/1

UNCLASSIFIED H W COLEMAN ET AL. JUN 87 AFOSR-TR-87-0895 F/G 20/13 NL

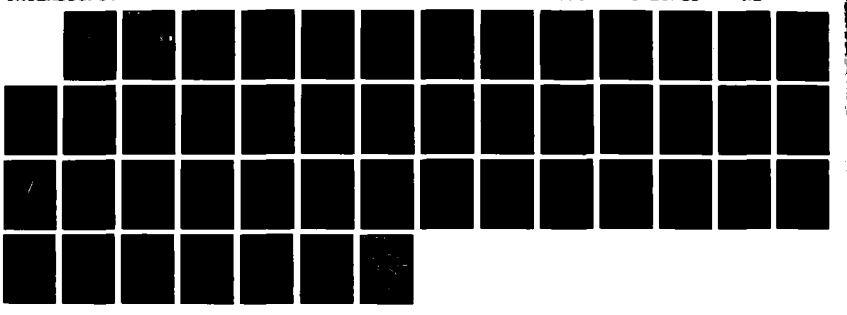

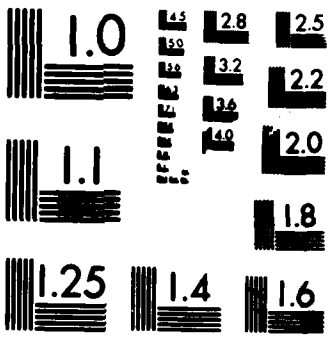

(2)

AFOSR-TR- 87-0895

An Experimental Study of Surface Roughness Effects on Turbulent Boundary Layer Flow and Heat Transfer

Hugh W. Coleman
Robert P. Taylor
Mechanical and Nuclear Engineering Department
Mississippi State University
Mississippi State, MS 39762

June 1987

Annual Technical Report for Research Grant AFOSR-86-0178
for Period 15 May 1986 - 14 May 1987

Prepared for

Air Force Office of Scientific Research
Bolling AFB, DC 20332-6448

ADA182913

REPORT DOCUMENTATION PAGE

1a. REPORT SECURITY CLASSIFICATION UNCLASSIFIED	1b. RESTRICTIVE MARKINGS
2a. SECURITY CLASSIFICATION AUTHORITY	3. DISTRIBUTION / AVAILABILITY OF REPORT Approved for public release; distribution unlimited.
2b. DECLASSIFICATION / DOWNGRADING SCHEDULE	
4. PERFORMING ORGANIZATION REPORT NUMBER(S)	5. MONITORING ORGANIZATION REPORT NUMBER(S) AFOSR-TR- 87-0895
6a. NAME OF PERFORMING ORGANIZATION Mech. & Nuc. Engr. Dept. Mississippi State University 6b. OFFICE SYMBOL (If applicable)	7a. NAME OF MONITORING ORGANIZATION Air Force Office of Scientific Research
6c. ADDRESS (City, State, and ZIP Code) P. O. Drawer ME Mississippi State, MS 39762	7b. ADDRESS (City, State, and ZIP Code) BCI 410 Bolling AFB, D.C. 20332-6448
8a. NAME OF FUNDING / SPONSORING ORGANIZATION Air Force Office of Scientific Research 8b. OFFICE SYMBOL (If applicable) AFOSR/NA	9. PROCUREMENT INSTRUMENT IDENTIFICATION NUMBER AFOSR-86-0178
8c. ADDRESS (City, State, and ZIP Code) BCI 410 Bolling AFB, D.C. 20332-6448	10. SOURCE OF FUNDING NUMBERS PROGRAM ELEMENT NO. 61102F; PROJECT NO. 2307; TASK NO. A1; WORK UNIT ACCESSION NO.
11. TITLE (Include Security Classification) An Experimental Study of Surface Roughness Effects on Turbulent Boundary Layer Flow and Heat Transfer	
12. PERSONAL AUTHOR(S) Coleman, Hugh W. and Taylor, Robert P.	
13a. TYPE OF REPORT Annual Technical 13b. TIME COVERED FROM 86MAY15 TO 87MAY14 14. DATE OF REPORT (Year, Month, Day) 87 JUNE 15. PAGE COUNT 46	
16. SUPPLEMENTARY NOTATION	
17. COSATI CODES FIELD / GROUP / SUB-GROUP	18. SUBJECT TERMS (Continue on reverse if necessary and identify by block number) Turbulent Boundary Layers Surface Roughness

19. ABSTRACT (Continue on reverse if necessary and identify by block number)

This annual technical report details the effort during the first year of this research program. The calibration and qualification of the Turbulent Heat Transfer Test Apparatus were completed for heat transfer measurements. The heat transfer data taken for zero pressure gradient, constant wall temperature, incompressible flow over a smooth wall agree with standard, accepted data sets for such conditions within the scatter of the standard data.

20. DISTRIBUTION / AVAILABILITY OF ABSTRACT ☒ UNCLASSIFIED/UNLIMITED ☐ SAME AS RPT. ☐ DTIC USERS	21. ABSTRACT SECURITY CLASSIFICATION UNCLASSIFIED
22a. NAME OF RESPONSIBLE INDIVIDUAL Dr. James D. Wilson	22b. TELEPHONE (Include Area Code) (202)767-4935 22c. OFFICE SYMBOL AFOSR/NA

DD FORM 1473, 84 MAR 83 APR edition may be used until exhausted. All other editions are obsolete.

TABLE OF CONTENTS

CHAPTER 1

OVERVIEW AND SUMMARY

1.1 Introduction

This annual technical report documents the first year's effort on the research program funded by Research Grant AFOSR-86-0178.

In this chapter the background on how this research program developed and why it is important is presented. This is followed by a discussion of the research objectives, the status of the research effort and other pertinent information. A description of the research facility and the experimental approach are presented in Chapter 2, and in Chapter 3 the preliminary baseline smooth wall heat transfer data are presented and compared with sets of standard, accepted Stanton number data. Details of calibrations and individual measurement uncertainties are presented in Appendix I, and an uncertainty analysis of the determination of Stanton number is presented in Appendix II.

1.2 Background

Given the geometry of an object immersed in a flowfield, a specification of the freestream flow conditions, and a geometrical description of the roughness of the system surfaces, the analyst or designer would like to be able at least to predict the surface shear distribution, the heat transfer distribution and the total drag. In the past most of the effort has been directed at the development of computational methods for various geometries with smooth surfaces, and the roughness problem has received relatively little attention. However, many systems of engineering interest have surfaces which are

aerodynamically rough. Therefore, if the flow parameters mentioned above are to be predicted, computational procedures to model the effects of rough surfaces must be developed and proven by comparison with well-documented data sets.

Schlichting (1936) experimentally investigated the fluid dynamics of this type of problem and related his skin friction results on a range of well-described rough surfaces to the previous results obtained by Nikuradse (1933) for sand-roughened pipes through definition of an equivalent sandgrain roughness, k_s. In subsequent surface roughness effects investigations, workers used these results of Schlichting and the equivalent sandgrain roughness concept in analyzing their experimental data and in developing analytical models for use in predictive methods. Over the years, several correlations were developed which produced a value of k_s for a rough surface when certain geometrical descriptors were known. These correlations were all intimately tied to the original k_s results of Schlichting.

Over the past decade or so, a predictive approach called the discrete element method, which does not use the equivalent sandgrain roughness concept, has been used with varying degrees of rigor by several groups of researchers. These efforts have used the original skin friction results of Schlichting to calibrate the roughness models in this method. This was necessary because the experimental results of Schlichting have remained the only data sets which included the effects of well-defined roughness element shape, size and spacing on skin friction.

During a recently completed research program funded by AFATL (Coleman, Hodge and Taylor, 1983) it was discovered that Schlichting had made erroneous assumptions during his data reduction which had significant effects on the data which he reported. The reevaluation of Schlichting's data (Coleman, Hodge and Taylor, 1984) showed that his skin friction results were too large by amounts ranging up to 73% and that his reported values of k_s were too high by amounts ranging from 26% to 555%. These findings caused some consternation since practically all work since the 1930's on surface roughness effects has relied significantly on either the skin friction or k_s results as originally reported by Schlichting.

In the present authors' work on the AFATL-sponsored research program, they derived from first principles a discrete element prediction approach for two-dimensional, nonisothermal turbulent boundary layer flow over a rough surface. The resulting equations are shown in Figure 1. Any such approach requires empirical input to calibrate the roughness model (much as empirical information was necessary to calibrate the turbulence models used in all Reynolds-averaged turbulent flow calculations). In this discrete element approach, experimental data are required to calibrate both a roughness element drag coefficient (C_D) model and a roughness element Nusselt number (Nu_D) model. The corrected data of Schlichting for surfaces with spherical, spherical segment and conical roughness elements of various size and spacing was used for the initial calibration of the C_D model. One heat transfer data set from the series of experiments at Stanford University

MASS:

$$\frac{\partial}{\partial x}(\rho\beta_{yz}u) + \frac{\partial}{\partial y}(\rho\beta_{xz}v) = 0$$

MOMENTUM:

$$\rho\beta_{yz}u\frac{\partial u}{\partial x} + \rho\beta_{xz}v\frac{\partial u}{\partial y} = -\frac{\partial}{\partial x}(\beta_{yz}P) + \frac{\partial}{\partial y}(\beta_{xz}\tau) - \rho C_D u^2 D(y)/2L\ell$$

ENERGY:

$$\rho\beta_{yz}u\frac{\partial h}{\partial x} + \rho\beta_{xz}v\frac{\partial h}{\partial y} = -\frac{\partial}{\partial y}(\beta_{xz}q) - (\beta_{xz}\tau)\frac{\partial u}{\partial y}$$

$$+ u\frac{\partial}{\partial x}(\beta_{yz}P) + \rho C_D u^3 D(y)/2L\ell$$

$$+ \pi\mu c(Nu)(T_R - T)/PrL\ell$$

Where: $\beta_{xz} = \beta_{yz} = (1 - \frac{\pi D^2(y)}{4L\ell})$, the blockage factor

$C_D = C_D(Re(y))$, the roughness element drag coefficient

$Nu = Nu(Re(y))$, the roughness element Nusselt number

$Re(y) = u(y)D(y)/\nu$, the local Reynolds number

$D(y)$ = roughness element diameter

L, ℓ = roughness element spacing in longitudinal and transverse directions

Figure 1. 2-D Compressible Turbulent Boundary Layer Equations Including Roughness Effects

(Healzer, 1974; Pimenta, 1975; Coleman, 1976) on a rough surface comprised of spheres of a single size packed in the most dense array has been used for the initial calibration of the Nu_D model.

As a result of the Air Force-sponsored research in the area, it became apparent that there is a critical need for highly accurate, precise and comprehensive data sets on both the heat transfer and the fluid dynamics in turbulent flow over well-defined rough surfaces. Recognition of this need led to the funding of the Turbulent Heat Transfer Test Facility (THTTF) at Mississippi State University under the DOD-University Research Instrumentation Program. This experimental facility is discussed in Chapter 2.

Most of the roughness-influenced turbulence data taken over the years has been on ill-defined rough surfaces, with the reported results having equivalent sandgrain roughness values implicitly included at some stage of the data reduction. As mentioned above, these k_s values of Schlichting are significantly in error and have finally been corrected forty years after they were reported. The Stanford data sets have been the only ones taken for a well-defined rough surface which contain heat transfer and skin friction distributions and velocity, temperature and Reynolds stress profiles; however, these data sets are for a single rough surface.

Holden (1983) has reported heat transfer and skin friction distribution measurements on well-defined surface roughnesses on cones, but the data were taken at hypersonic flow conditions. In a program currently funded by AFWAL, the authors are determining skin friction coefficients in fully developed pipe flows with well-defined surface

roughnesses. These experiments cover the effects of roughness size, shape and spacing on friction coefficient. They should be completed by September, 1987.

It was concluded that if the need for comprehensive data sets for turbulent flow over rough surfaces is to be satisfied, if a reasonable predictive capability is to be developed, and if an increased understanding of the physics of the interactions between surface roughness and turbulence is to be achieved, then experimental information (particularly on heat transfer) in addition to that in the efforts mentioned above must be obtained. The current research program is intended to provide very accurate and precise measurements of Stanton number and skin friction distributions and profiles of velocity, temperature and Reynolds stresses in turbulent boundary layer flows over surfaces roughened with well-defined roughness elements and to lead to improved predictive capabilities for turbulent flows over rough surfaces.

1.3 Research Program Objectives

This research program is intended to obtain heat transfer and fluid dynamic data from incompressible turbulent boundary layer flows in the aerodynamically smooth, transitionally rough and fully rough regimes over a range of well-defined rough surfaces. These data will be used to improve and extend the roughness models in the previously discussed discrete element approach for turbulent flow over rough surfaces. The experimental data obtained will thus immediately be used to enhance and expand the capability to predict the effects of surface roughness on turbulent flow and heat transfer.

The experimental conditions to be run and the rough surfaces to be used were chosen based on the following criteria:

(a) the tests should provide the maximum information for the time, effort and money expended

(b) the range of the results should complement (and overlap when possible) the rough surface data from the Stanford experiments, the corrected Schlichting data and the data from the current fully-developed flow investigation using the water tunnel at Mississippi State University, and

(c) the data should cover the aerodynamically smooth, transitionally rough and fully rough flow regimes.

To have an experimental data base which is minimally adequate for researchers attempting to describe the interaction of surface roughness and turbulent flow and to develop useful predictive models for a wide range of flow conditions, the authors believe comprehensive experiments should be run for a baseline smooth surface and for surfaces with hemispherical elements spaced 2, 4 and 10 diameters apart, conical elements spaced 2, 4 and 10 base diameters apart, a "quasi-random" mixture of hemispherical and conical elements at two different average spacings, and a random pattern corresponding to a "real" case. Such a number of different test surfaces is, of course, well beyond that which can be experimentally investigated in a careful and meaningful manner in a two year research program.

The University Research Instrumentation Program (URIP) grant which funded the acquisition of equipment and construction of the THTTF did not provide for any research use of the facility. It essentially funded the facility up to the point where it was completely assembled

and first turned on. The first objective of this research program, then, is the calibration, qualification and general "shake-down" of the facility with a smooth test surface. The ability to reproduce accepted smooth wall results for nonisothermal turbulent boundary layer flow in the THTTF should be demonstrated before proceeding with any rough wall investigations using the facility. In addition, smooth wall data from the same facility will be an appropriate baseline with which to compare the data from rough wall flows.

Once acceptable smooth wall results are obtained, it is planned that the sets of surfaces roughened with hemispherical elements and conical elements will be used in sequential investigations. Five sets of test plates (the smooth, the three with hemispherical elements and one with conical elements) were obtained for the test facility under the URIP grant. The grant for the current two-year research program included funds to obtain the other two sets of test plates with conical elements.

The THTTF has been designed so that the 24 test surface plates can be replaced with a new set without completely tearing down the test section. Some re-instrumentation, calibration and qualification will be necessary for each new set of test surface plates, however, to maintain the high accuracy and precision which are an inherent part of the overall objective of this test program.

The experimental plan is to test each surface with boundary conditions of zero pressure gradient and constant wall temperature over a number of freestream velocities between about 6 m/sec and 60 m/sec such that the total set of data will thoroughly cover behavior in the aerodynamically smooth, transitionally rough and fully rough regimes.

Probably the most important data will be the heat transfer (Stanton number) distributions, since the only such data currently available on a well-described rough surface are those from the Stanford experiments for a single rough surface composed of spheres packed in the most dense array. In addition to the Stanton numbers, skin friction coefficient distributions will be determined and profiles of temperature, velocity and Reynolds stress components will be measured.

It was anticipated that the calibration, qualification and general shake-down of the THTTF with the smooth test surface would take from 9 to 15 months and that 4 to 8 months would be required to install each new test surface and obtain the experimental data desired.

1.4 Status of the Research Effort

Calibration, qualification and shake-down of the facility (with smooth walls) is nearing completion for heat transfer measurements. Comparisons of measured Stanton number distributions with the standard data sets and correlation for smooth walls are presented and discussed in Chapter 3. Details of calibrations are presented in Appendix I, and the uncertainty analysis of the Stanton number determinations is presented in Appendix II.

An alignment jig for the hot wire and thermocouple probes has been designed and built, and initial work with the hot wire probes is underway. Once calibration procedures for the hot wire anenometer system have been completed successfully, measurements of profiles of mean velocity and Reynolds stress components and distributions of skin friction coefficients will be made and compared with reference smooth wall data.

The schedule of the research program has been adversely impacted by between one and two months due to the complete renovation of the power service and the HVAC systems in Patterson Laboratory, which is the building which houses the test facility. This was beyond the control of the principal investigators. However, this will have a positive effect on the research programs which use the THTTF. The old power service in the building was outdated, overloaded and unreliable.

One final point which should be noted is the status of the manufacture of the rough test plates. As mentioned previously, the URIP grant contained funds for the set of smooth test plates and four sets of rough plates, and this research grant contains funds for the fifth and sixth sets of rough plates. A bid by Hye Precision Products Corp. of Perry, Georgia to manufacture the plates was accepted, and they successfully delivered the smooth set. They had planned to cold form the plates with roughnesses on the surface, but this technique was unsuccessful. Efforts at forming using heated aluminum blanks and using powdered aluminum were likewise unsuccessful. They have decided to machine the plates using a numerically-controlled machine and are currently working on the cutter design so that a satisfactory surface finish is achieved. They are confident that the rough plates can be manufactured to meet the specifications using their NC-machine. The delay in delivery of rough plates has not yet impacted the research program, since initial work was all planned with the smooth wall test plates.

1.5 Other Pertinent Information

The professional personnel participating in the research program are the two principal investigators, Professors Hugh W. Coleman and Robert P. Taylor. Two M.S. students, Mr. G. B. Brown and Mr. W. F. Scaggs, are involved in the program and anticipate completing their M.S. programs in December 1987. Mr. M. H. Hosni is the doctoral student working on the program. He began his Ph.D. program in the fall of 1986.

CHAPTER 2

DESCRIPTION OF FACILITY AND EXPERIMENTAL APPROACH

The Turbulent Heat Transfer Test Facility (THTTF), shown schematically in Figure 2, is a closed-loop system designed to deliver a uniform velocity (6 to 60 m/sec), low turbulence intensity, controlled-temperature air flow at the 10.2 by 50.8 cm (4.0 by 20.0 in) inlet of the 2.4 m (8.0 ft) long test section. This corresponds to an x-Reynolds number range of about one million to ten million at the end of the test section. The bottom surface of the test section is composed of 24 test plates, each with its own power supply/control circuit and temperature instrumentation. The upper surface of the test section is a flexible 1.3 cm (0.5 in) thick sheet of clear cast acrylic which can be adjusted to maintain a prescribed pressure gradient along the flow direction. A Hewlett-Packard 3054S Automatic Data Acquisition and Control System (ADACS) is used for controlling the apparatus, maintaining set points, and acquiring and reducing the data.

Air velocity in the test section is set using an Eaton eddy clutch controller to control the rotation speed of the blower. The controller can be adjusted and set using a manually-adjusted potentiometer or a dc-voltage signal from the ADACS. From the blower, the air flow travels through an overhead duct, passes through a linen cloth filter, a 4-row cooling coil, a section of honeycomb and screens, and a 19.8 to 1 contraction nozzle into the test section. Preliminary measurements at

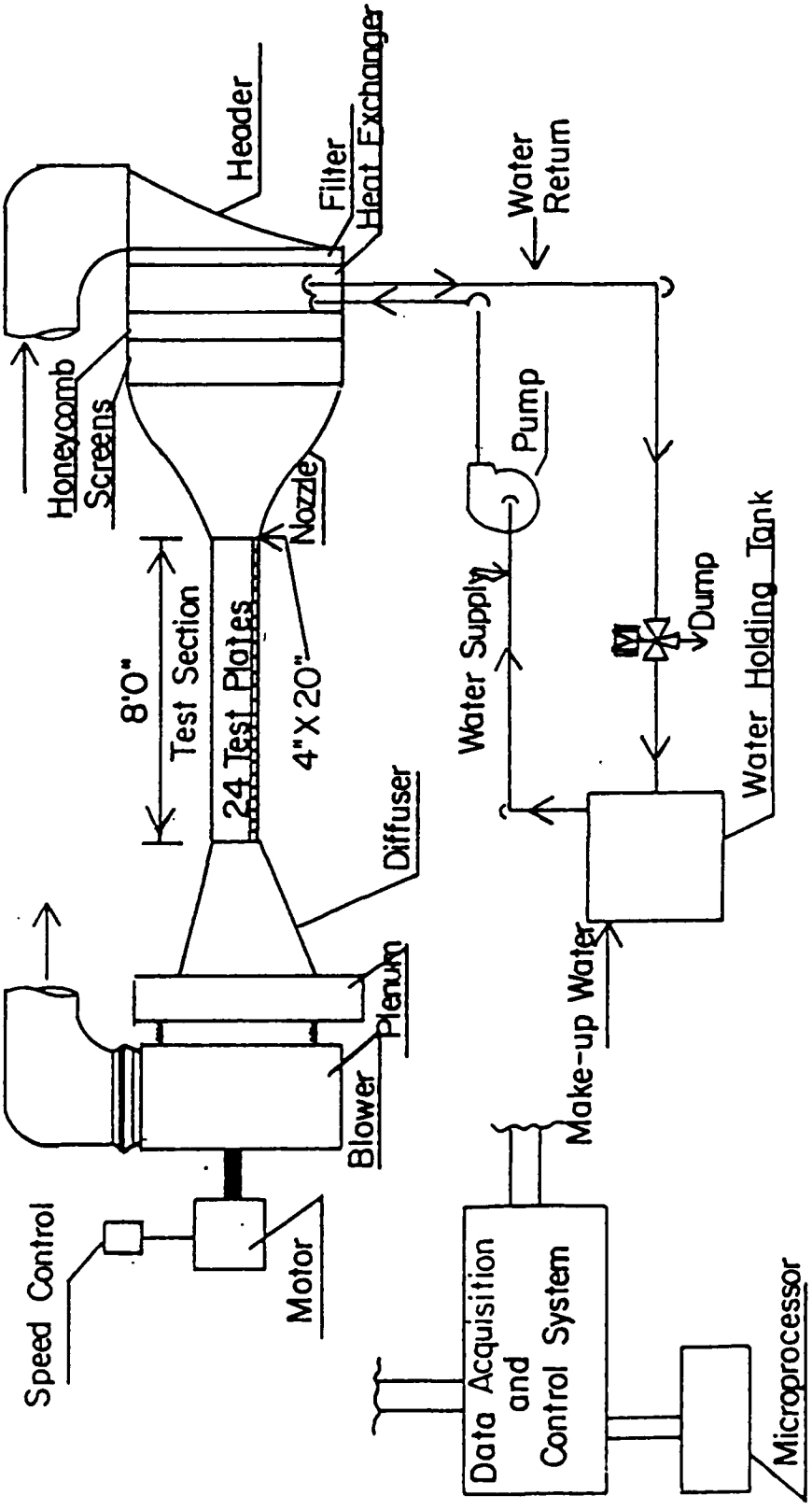

Figure 2. Schematic of the Turbulent Heat Transfer Test Facility (THTTF).

freestream air velocities of 12 and 27 m/sec indicate the flow at the nozzle exit is uniform within about ± 0.5% with a turbulence intensity of less than 0.5%.

The 24 plates which comprise the test surface are each 10.2 cm (4.0 in) in the flow direction by 45.7 cm (18.0 in) in the transverse direction by 0.95 cm (0.375 in) thick. The test plates are made of electroless nickel plated aluminum, and the smooth surface plates which are being used in the baseline tests have a surface finish which has been measured as less than 20 microinches. The plates are assembled using dowels as shown in Figure 3 to form the test surface. The allowable step (or mismatch) at the joint between two plates is 0.0013 cm (0.0005 in). Each plate is instrumented with two thermistors for temperature measurement, and each has its own motor-driven variable voltage transformer/plate heater circuit which is controlled by the ADACS. Experience in acquiring the heat transfer data presented in Chapter 3 has shown that plate temperatures can be held within ± 0.1°C of a prescribed constant temperature boundary condition along the entire test section.

A cross section view of the test section is shown in Figure 4. The test plates are supported on precision straightedges which are thermally isolated from the steel side rails which provide the primary structural support. These side rails are heated, so that they act as guard heaters and thus help to minimize the conduction heat losses from the plates.

Heat transfer (Stanton number) distributions along the test surface are determined from energy balances on each of the plates, taking into account conduction and radiation heat transfer losses. As

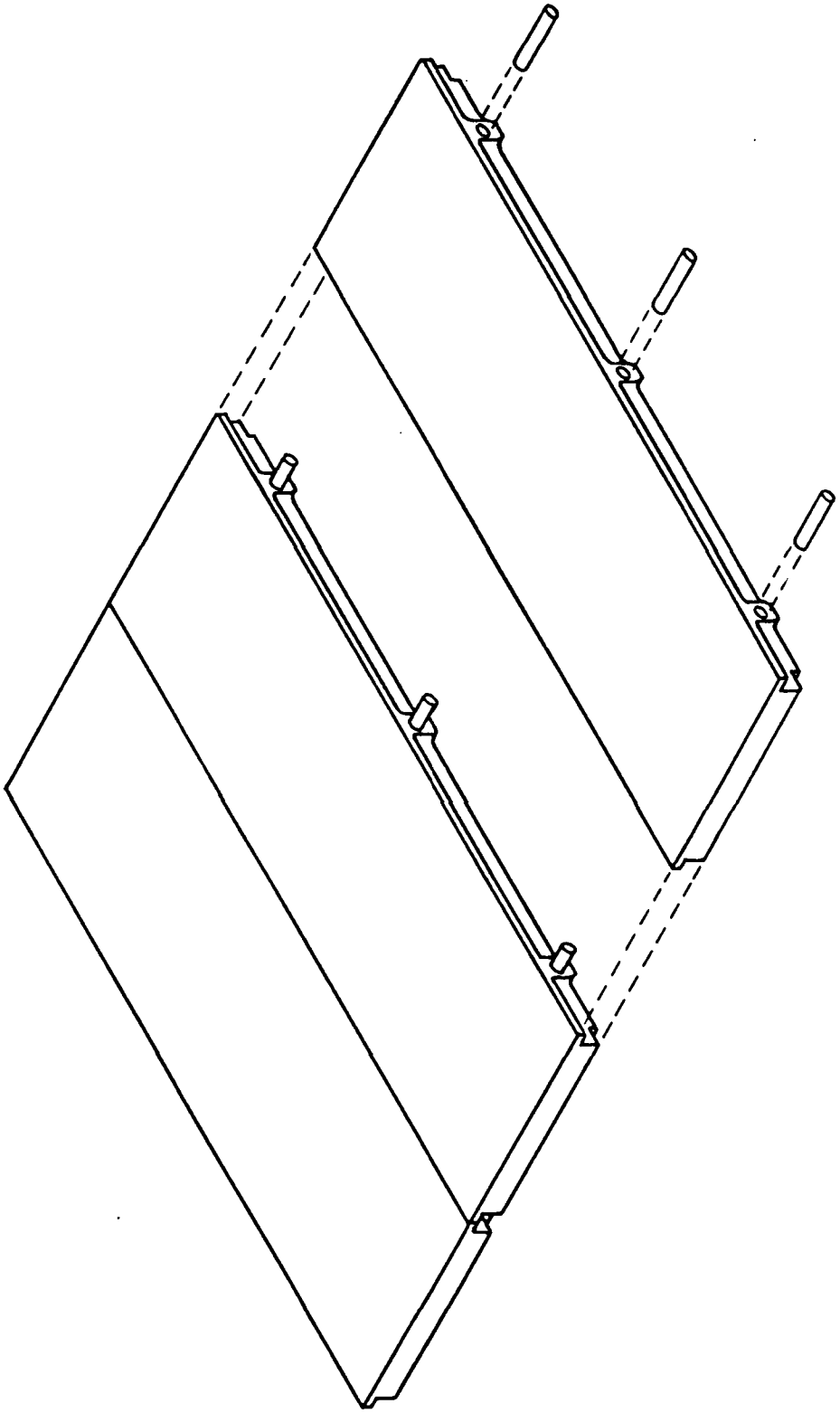

Figure 3. Smooth Test Plate Assembly.

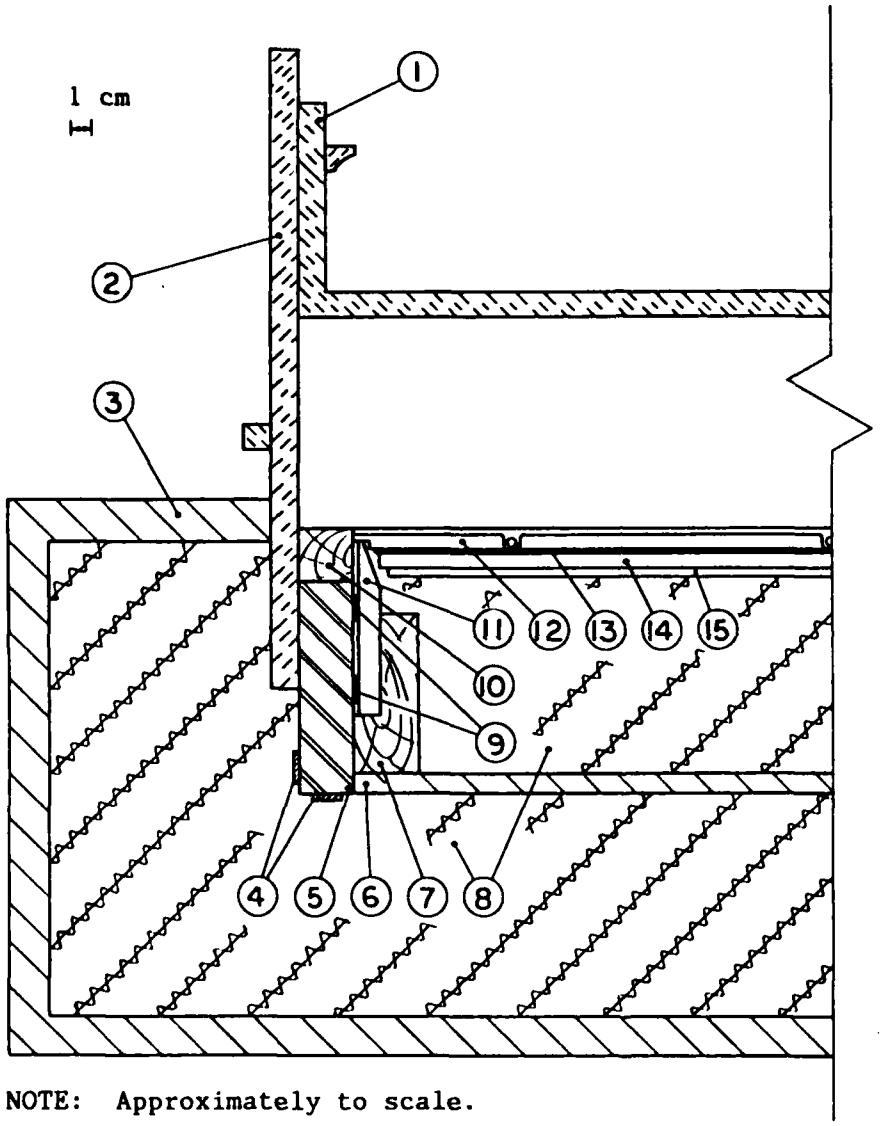

1. Top Wall Assembly
2. Tunnel Side Wall
3. Wooden Housing
4. Side Rail Heaters
5. Steel Side Rail
6. Wooden Section Closure
7. Wooden Beam
8. Thermal Insulation
9. Birch Strips
10. Balsa Strip
11. Precision Straightedge
12. Aluminum Test Plate
13. Heater Pad
14. Insulation Pad
15. Aluminum Backing Plate

NOTE: Approximately to scale.

Figure 4. Cross Section of the THTTF Test Section.

discussed in Appendix II, an uncertainty analysis indicates that Stanton numbers can be determined within about 3% in the THTTF using this approach.

Boundary layer temperature profiles will be measured with a butt-welded cylindrical thermocouple probe calibrated against a quartz thermometer as discussed in Appendix I.

Boundary layer mean velocity and turbulence profiles will be measured using a TSI IFA-100 anemometer unit and Dantec horizontal boundary layer and 45-degree slant hot wire probes. Distributions of skin friction coefficient will be determined from the hot wire measurements of Reynolds shear stress as described by Coleman, Moffat and Kays (1977).

CHAPTER 3

PRELIMINARY HEAT TRANSFER DATA

The objective of this section is to compare the smooth wall Stanton number measurements on the THTTF with data from other respected sources. The purpose of this comparison is to document the correctness of the instrumentation, the data acquisition system, and the data reduction procedures used in obtaining the heat transfer data on the THTTF. All comparisons given here are for zero pressure gradient, constant wall temperature, incompressible boundary layer flow without transpiration. The boundary layer was tripped turbulent at the leading edge of the test surface.

The definitive data sets for the conditions of interest are those of Reynolds, Kays and Kline (1958). In fact, these are the only widely referenced data for the conditions of interest and serve as the basis for all heat transfer correlations for these conditions. They are the only data quoted for these conditions by such well known references as Kays and Crawford (1980) and Rohsenow and Hartnett (1973). Their experimental apparatus consisted of 24 individually heated copper plates. The plate dimensions were 6.4 cm (2.5 in) long in the flow direction by approximately 84 cm (33 in) wide. This gave a total surface length of 1.5 m (60 in). This test surface was placed in a 2.3 m (7.5 ft) free-jet wind tunnel with free stream turbulence intensity of between 2 and 5 percent. Stanton numbers were determined by measur-

ing the power input to each plate and the temperature difference between the plate and free stream and correcting for heat losses. Figure 5 shows a plot of this data along with the correlation

$$St = .0286\ (Re_x)^{-0.2}(Pr)^{-0.4} \qquad (1)$$

suggested by Moffat (1967) and the +5 percent and -5 percent bands about Eq. (1). Inspection of the figure reveals that most of the data scatter within the ± 5 percent band. The data in this figure represent 8 individual runs with free stream velocities ranging from 13.9 m/s (43 ft/s) to 38.7 m/s (127 ft/s).

The next data sets which were chosen for comparison are from a series of experiments at Stanford University. The data sets used here come from Moffat (1967), Kearney (1970) and Orlando (1974). These experiments were mainly concerned with the effects of transpiration on heat transfer in the turbulent boundary layer. Their surface was porous to allow transpiration but had an rms roughness of 200 micro-inches, which proved to be aerodynamically smooth at the low velocities used in the experiments. Each of the workers took baseline non-transpired data to qualify the experimental apparatus, and it is this data which is of interest. All of these experiments were conducted on a test facility which was very similar to the THTTF. The test bed consisted of 24 individually heated plates. Each plate was 10.2 cm (4.0 in) long by 45.7 cm (18 in) wide, resulting in a 2.4 m (8.0 ft) long test bed. The nominal free stream turbulence was 0.7 percent. Stanton numbers were determined by measuring the plate and free stream temperatures and the power input to each plate and correcting for heat losses. Seven data sets were selected to represent the early, mid and late time periods of the series. Figure 6 shows a plot of the data

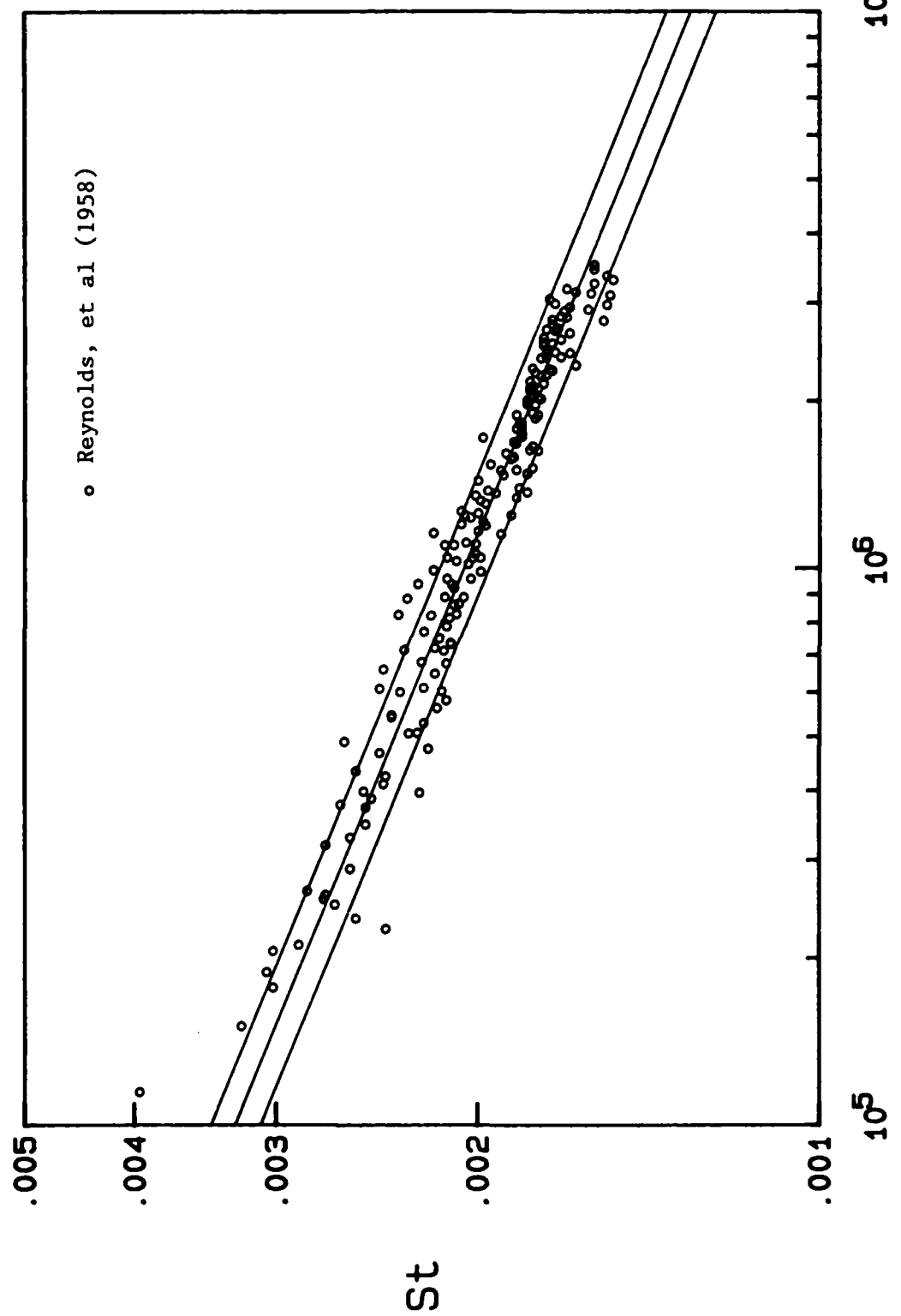

Figure 5. Stanton Number Data of Reynolds, Kays and Kline (1958) Compared with the Correlation of Eq. (1).

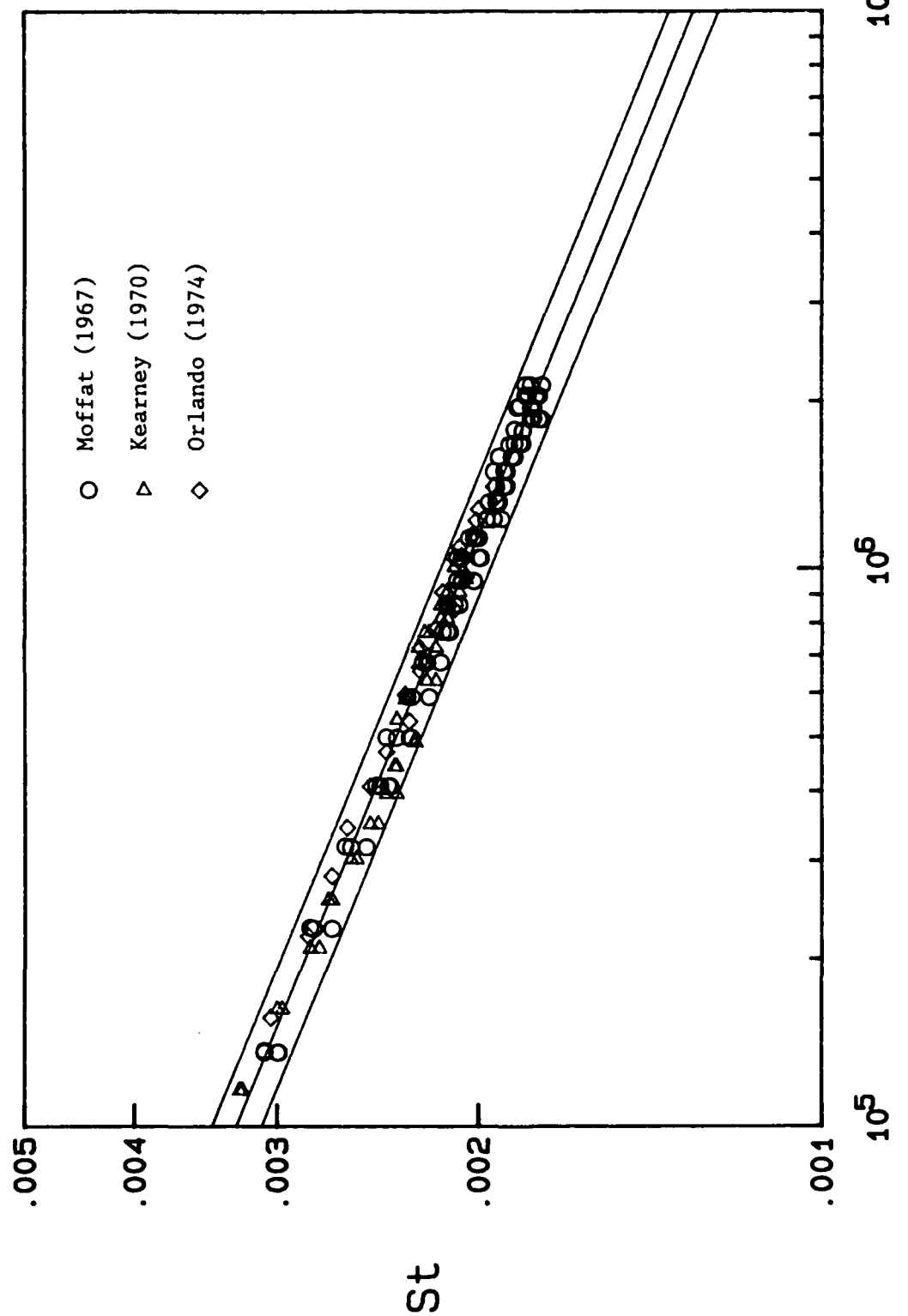

Figure 6. Stanton Number Data of Moffat (1967), Kearney (1970), and Orlando (1974) Compared with the Correlation of Eq. (1).

along with Eq. (1) and the ±5 percent bands. Inspection of the figure reveals that the data all scatter within the ±5 percent bands. These data represent free stream velocities ranging between 7 m/s (23 ft/s) and 13.4 m/s (44 ft/s).

The comparisons above demonstrate that Eq. (1) is a reasonable approximation of the existing smooth wall, constant temperature, zero pressure gradient Stanton number data and that the existing data scatter within approximately ±5 percent about this correlation. Therefore, if the present data are within ±5 percent of Eq. (1), it can be concluded that the calibration and qualification of the THTTF has been successfully completed for heat transfer measurement.

Figure 7 shows a plot of the present data along with the correlation of Eq. (1) and the ±5 percent bands. Inspection of the figure reveals that the data are almost all within the ±5 percent bands. The present data sets cover a larger Reynolds number range than the previous data (Re_x = 6 x 10^6 versus 3 x 10^6) and a larger range of free stream velocities. The 12.0 m/s (39.4 ft/s) free stream velocity data agree almost exactly with the correlation of Eq. (1), which was developed by Moffat (1967) from data taken at 13.4 m/s (44 ft/s).

Figure 8 shows a composite plot of all the data considered in this comparison. Inspection of the figure reveals that the present data agrees with the previous data within the scatter of the data sets as a whole. Therefore, it can be concluded that the preliminary Stanton number data from the THTTF is in substantial agreement with standard data and that the facility is operating correctly for heat transfer measurements.

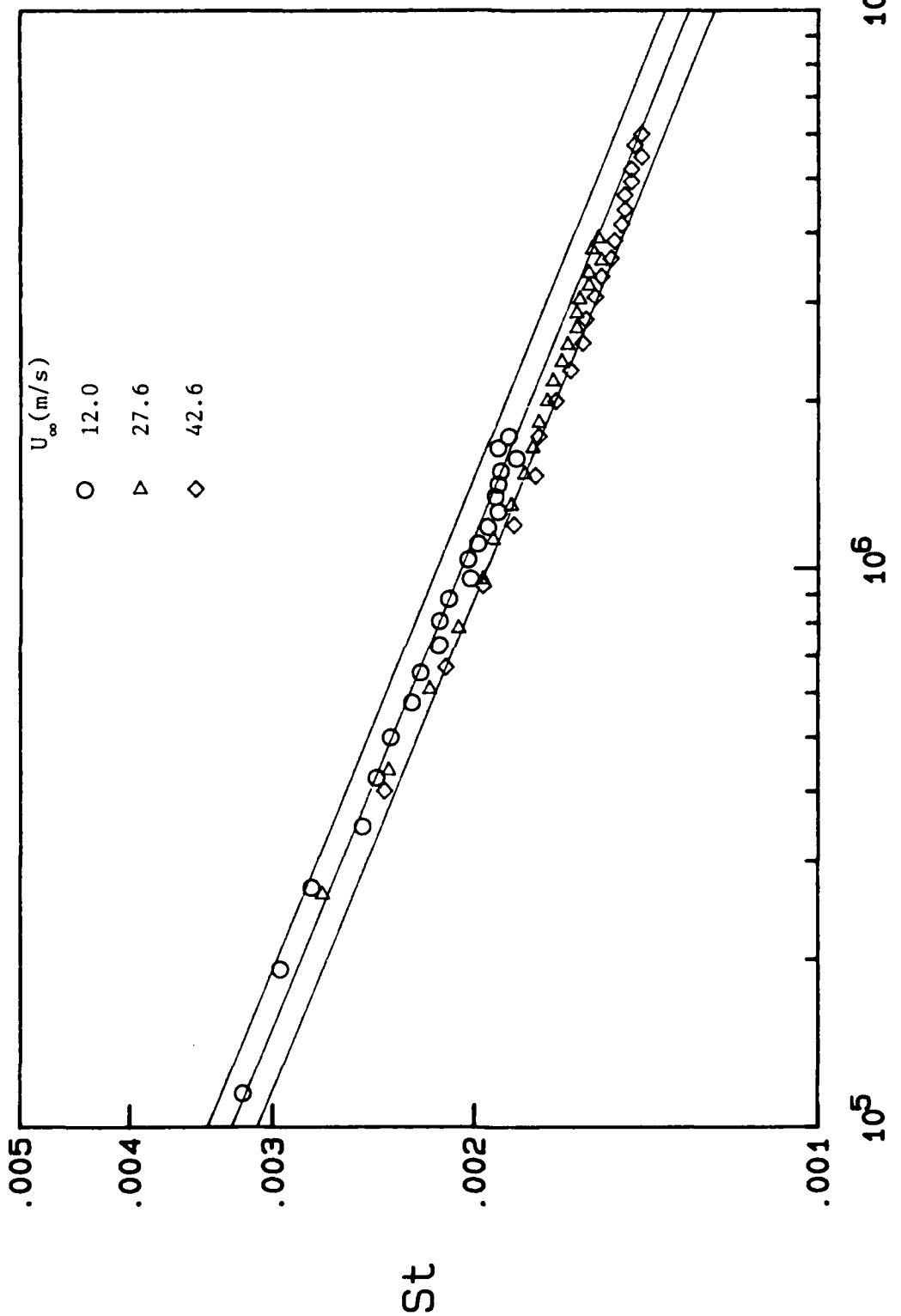

Figure 7. Stanton Number Data of the Present Experiments Compared with the Correlation of Eq. (1).

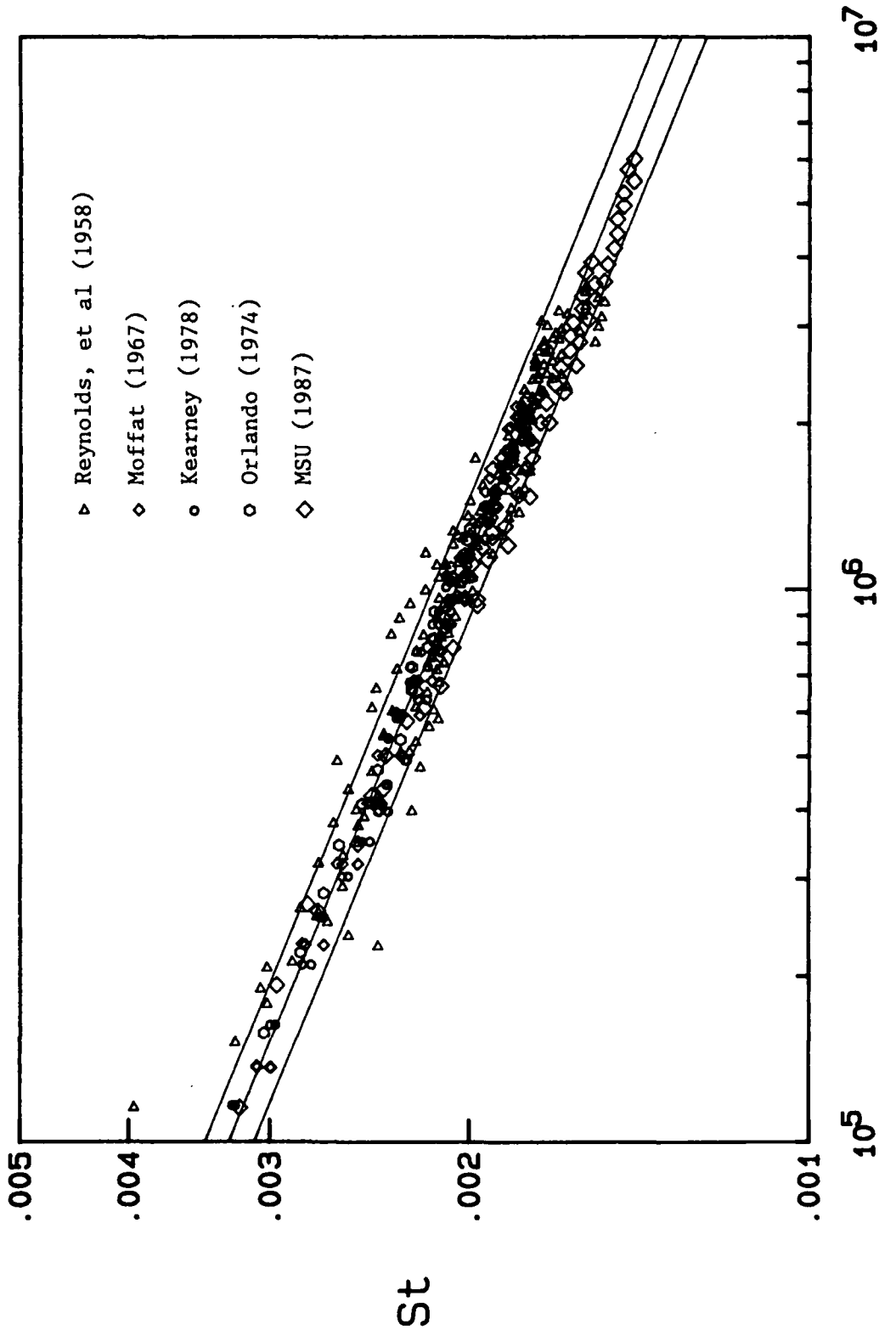

Figure 8. Composite Plot of All of the Stanton Number Data Considered in This Comparison.

REFERENCES

Coleman, H. W. 1976: Momentum and energy transport in the accelerated fully rough turbulent boundary layer. Ph.D. Dissertation, Mech. Eng. Dept., Stanford Univ.

Coleman, H. W.; Hodge, B. K.; Taylor, R. P. 1983: Generalized roughness effects on turbulent boundary layer heat transfer. AFATL-TR-83-90.

Coleman, H. W.; Hodge, B. K.; Taylor, R. P. 1984: A reevaluation of Schlichting's surface roughness experiment. Journal of Fluids Engineering, Vol. 106.

Coleman, H. W.; Moffat, R. J.; Kays, W. M. 1977: The accelerated fully rough turbulent boundary layer. J. Fluid Mechanics, Vol. 82, Part 3.

Healzer, J. M. 1974: The turbulent boundary layer on a rough, porous plate: Experimental heat transfer with uniform blowing. Ph.D. Dissertation, Mech. Eng. Dept., Stanford Univ.

Holden, M. S. 1983: Studies of surface roughness effects in hypersonic flow. Calspan Report No. 7018-A-2.

Kays, W. M.; Crawford, M. E. 1980: Convective heat and mass transfer. McGraw-Hill Book Co., New York.

Kearney, D. W. 1970: The turbulent boundary layer: Experimental heat transfer with strong favorable pressure gradients and blowing. Ph.D. Dissertation, Mech. Eng. Dept., Stanford Univ.

Moffat, R. J. 1967: The turbulent boundary layer on a porous plate: Experimental heat transfer with uniform blowing and suction. Ph.D. Dissertation, Mech. Eng. Dept., Stanford Univ.

Orlando, A. F. 1974: Turbulent transport of heat and momentum in a boundary layer subject to deceleration, suction and variable wall temperature. Ph.D. Dissertation, Mech. Eng. Dept., Stanford Univ.

Nikuradse, J. 1933: Stromungsgesetze in rauhen rohren. VDI-Forchungsheft 361. (Also Laws of flow in rough pipes. NACA TM 1292.)

Pimenta, M. M. 1975: The turbulent boundary layer: An experimental study of the transport of momentum and heat with the effect of roughness. Ph.D. Dissertation, Mech. Eng. Dept., Stanford Univ.

Reynolds, W. C.; Kays, W. M.; Kline, S. J. 1958: Heat transfer in the turbulent incompressible boundary layer-constant wall temperature. NASA memorandum 12-1-58W, Washington.

Rohsenow, W. M.; Hartnett, J. P. 1973: Handbook of heat transfer. McGraw-Hill Book Co., New York.

Schlichting, H. 1936: Experimentelle untersuchungen zum rauhigkeits-problem. Ingenieur-Archiv. Vol. VII, No. 1, pp. 1-34. (Also Experimental investigation of the problem of surface roughness. NACA TM 823).

APPENDIX I

CALIBRATIONS AND INDIVIDUAL MEASUREMENT UNCERTAINTIES

1. Temperature

(a) Thermistors

Temperatures are measured using Fenwal Electronics UUT45J1 thermistors which are temperature sensitive resistors with a negative temperature coefficient. These thermistors have a nominal resistance of 50000 ohms at 25°C and are highly sensitive to small temperature changes (about 1-2 KΩ/°C). They are guaranteed, by the manufacturer, to have ±0.2°C interchangability over a standard range of temperatures from 0°C to 70°C. The resistances of the thermistors are measured by the Hewlett Packard Model 3054 Automated Data Acquisition and Control System (ADACS).

The calibration of the thermistors was done in a Blue M Model MR-3210A-1 constant temperature bath. The bath temperature was monitored by a Hewlett Packard Model 2804A quartz thermometer instrumented with Model 18111A quartz probe. The absolute accuracy of this thermometer probe combination, specified by HP, is ±0.040°C over a range of -50 to 150°C. Its calibration was checked by placing the probe into a standard stirred ice bath and verifying its reading of 0.000°C. The thermistors were placed individually inside glass test tubes to protect them and avoid their contamination. To insure effective conduction of heat from the water bath to each thermistor, each test tube was filled with Omegatherm 201 (by Omega Engineering, Inc.) which is a very high thermal conductivity, filled silicone paste. The spatial variation in the temperature of the bath was found to be about ±0.4°C. This varia-

tion was minimized to ±0.02°C by centering the test tubes containing thermistors around the quartz probe in groups of fourteen. Since the reliability of measured thermistor resistances depends on the accuracy of measurements made by the ADACS, the proper use of the ADACS during the measurement process was carefully examined.

The thermistor calibrations were performed for the range of temperatures 22°C-50°C using six evenly spaced points over this range. The thermistors are extremely nonlinear but can be very closely approximated by the Steinhart-Hart equation as

$$T[°K] = 1/[A + B \ln R + C(\ln R)^3]$$

where R is resistance in ohms. The curvefit constants A, B and C were calculated using the thermistor manufacturer's data and are $A = 9.6401 \times 10^{-4}$, $B = 2.1095 \times 10^{-4}$ and $C = 8.48 \times 10^{-8}$.

The temperatures obtained using the measured thermistor resistances in the Steinhart-Hart relation were compared with the temperatures from the quartz thermometer. The difference between the temperatures measured by the quartz thermometer and the temperatures calculated from the measured thermistor resistances using the curvefit equation was determined for a total of 360 calibration points. Figure I-1 shows the cumulative probability curve of the absolute values of the temperature differences. As shown, 95% of the temperature differences are less than about 0.09°C. Such a calibration result was obtained after more than 14% of the original thermistors were replaced. It should be emphasized that such replacements required recalibration of the entire group of thermistors. This indicates the extent of time spent on the thermistor calibrations.

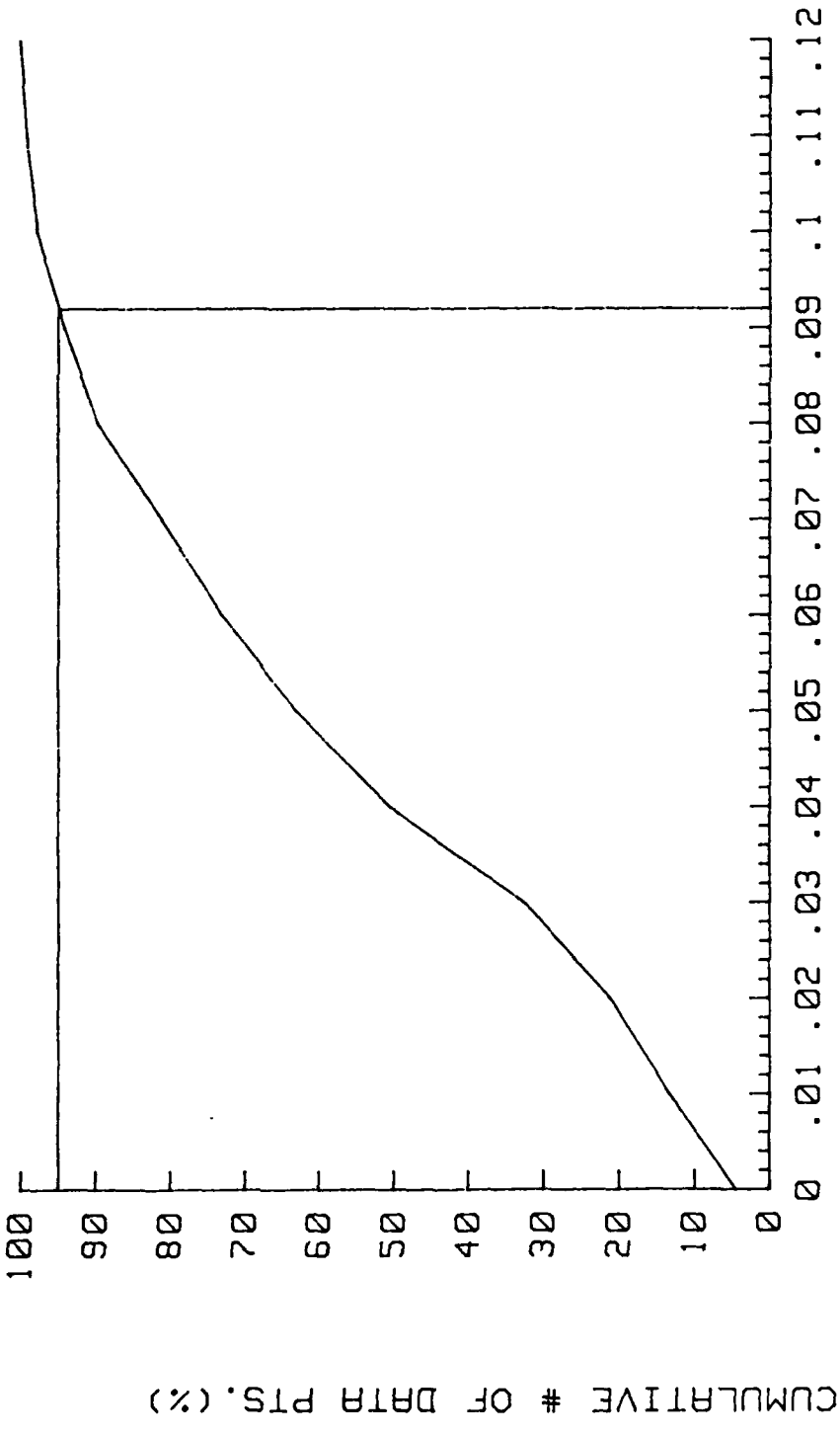

Figure I-1. Thermistor Calibration Results.

(b) Thermocouple Probe

The boundary layer temperature is measured using a type E (Chromel-constantan) thermocouple probe. The output of the thermocouple is in the millivolt range and is measured by the ADACS.

The calibration was done in the Blue M Model MR-3210A-1 constant temperature bath, and the Hewlett-Packard quartz thermometer described earlier was utilized to measure the bath temperature. The calibration water bath was in continuous movement due to an automatic stirrer facility, and the risk of breaking the fine thermocouple wire was large if the probe was placed directly into it. Besides, water could deposit some residue on the wire surface and the prongs, which could influence the thermocouple temperature response. Moreover, the water temperature close to the thermocouple could not be accurately monitored by the quartz thermometer. To alleviate those difficulties it was decided to insert the wire into a jar filled with alcohol, which was placed in the water bath. The quartz thermometer was also positioned in the jar next to the thermocouple probe so that it would encounter the same conditions. To prevent any air current from convecting heat from or to the alcohol surface, the opening of the jar was sealed. The time constant of the jar was also accounted for by proceeding with the temperature measurement an hour after the water bath temperature had reached the steady state condition.

Calibration was performed for temperatures between 23°C-39°C using four points over this range. The thermocouple probe voltage outputs, as measured by the ADACS, were converted to temepratures using the HP system software package. The temperature of the reference junction (the isothermal terminal block) required for software compensation is

established by the ADACS via a temperature transducer which provides a 100 mV/°C output voltage. This software performs the voltage-temperature conversion by dividing the thermocouple characteristic curve into eight sectors and approximating each sector by a third order nested polynomial. The temperatures measured by the thermocouple were compared with the temperatures from the quartz thermometer over the above mentioned calibration range. The departure of thermocouple temperatures, using the software package for conversion, from the corresponding temperatures obtained by the quartz thermometer was less than ±0.08°C.

2. Power

Power measurement is one of the most important tasks among the various measurements. Its accuracy plays a major role on the reliability of the experimental results. The power measurement was performed using a high precision A.C. watt transducer, Ohio Semitronics Inc. Model EW5-B, which the manufacturer specifies to have ±0.2% of reading accuracy and 0 to 1 ma current output proportional to electrical power. This model is a single phase transducer and the rated output of 1 ma corresponds to 500 watts.

The ADACS was used to measure the transducer output. Since the ADACS can not process current signals directly, the watt transducer output was measured indirectly. A 5.5 KΩ resistor was shunted across the watt transducer output lines so that the current output was transformed into a measurable voltage. The shunt resistor was sized to compensate for the small current output from the watt transducer.

Power is supplied to 24 test plate heaters and one power measurement calibration plate heater through identical power circuits. The line voltage applied to all plate heater circuits is fed through an A.C. voltage regulator. This insures the consistency of the line voltage and prevents significant temporal variations in plate heater powers. Manual and motor actuated variable voltage transformers connected in series are applied to set the power (voltage) to each of the plate heaters. The transformers positions are kept fixed during each power measurement and, hence, the stability of the power during the measurement process is insured.

The watt transducer calibration was accomplished by comparing the transducer measurement to the actual calibration plate heater power input which was measured using the ADACS as described below. For the transducer measurement the watt transducer was engaged in the plate heater power circuit using automated switch closures. Its current output, which corresponds to the power, was introduced through the shunt resistor. The D.C. voltage drop across this resistor and its resistance were measured by the ADACS.

The actual power, on the other hand, was obtained by measuring the A.C. voltage drop across the plate heater and the resistance of the plate heater and subsequently substituting into

$$P_{actual} = \frac{V^2}{R}$$

Due to the importance of resistance and voltage measurement in determination of both transducer and actual powers, extreme care was exercized to utilize the ADACS properly and efficiently. In particular, the plate heater and shunt resistors were measured using

the four-wire technique. In this method, the resistance of the transmission line is measured and is subtracted from the measured total resistance automatically. Therefore, the resistance obtained by the four-wire technique represents the load resistance alone. The uncertainties in the resistance and voltage measurements using the ADACS are specified by HP to be less than 0.001% and 0.003% of reading, respectively. These are so small that, for all practical purposes in this experimental investigation, they are assumed to be zero.

The power indicated by the output of the watt transducer was compared with the actual power as measured by the ADACS using 115 points over the 0-250 watt range of interest. A 95% confidence estimate of the uncertainty in the watt transducer power measurement based on these points is ±1.0 percent of reading.

3. Pressure

Pressure measurement is performed using two differential pressure transducers, both Validyne Model P305D, with ranges of 0.08 psi and 0.5 psi. These transducers cover the full range of pressures expected. Their accuracy, specified by the manufacturer, is ±0.5 percent of full scale. Each transducer provides a voltage output of 0-5 Vdc proportional to the applied pressure difference. The voltage outputs of the pressure transducers are measured by the ADACS.

The calibration of each pressure transducer was accomplished by employing a very sensitive water micromanometer, Meriam Instruments Model 34FB2TM, as the pressure source. The 10" micromanometer is

equipped with a magnifier to amplify the fluid meniscus at the reference hairline which provides direct reading indication of 0.001" of water.

Each pressure transducer was calibrated individually. Various pressures within the pressure transducer range were generated using the micromanometer and were applied to the transducer. The values of these generated pressures indicated by the micromanometer and the corresponding voltage outputs from the pressure transducer were recorded. The number of pressure calibration points obtained for the 0.08 psi and 0.5 psi range transducers were 23 and 10, respectively. Both pressure transducers demonstrated small but stable voltage outputs at zero pressures (zero shift). The pressure calibration data collected from each transducer was compensated for the zero shift.

Subsequently, the corrected data of each transducer was used to arrive at an appropriate curvefit equation for that transducer. A linear curvefit equation for the 0.5 psi range pressure transducer was satisfactory, but a quadratic equation was necessary to fit the 0.08 psi range pressure transducer calibration data satisfactorily.

A comparison between the direct pressure measurement data (micromanometer readings) and the pressures calculated from the curvefit equation was made for each pressure transducer. The results indicated that the measurement uncertainties of the 0.08 psi and 0.5 psi range transducers were ±0.5 percent and ±0.1 percent of reading, respectively.

APPENDIX II

UNCERTAINTY ANALYSIS OF STANTON NUMBER DETERMINATION

The final data reduction expression for the experimentally determined Stanton number is

$$St = \frac{w - q_r - q_c}{A\rho C_p U_\infty (T_p - T_\infty)} \qquad \text{(II-1)}$$

where

w is power into the plate heater

q_r is radiation loss from plate

q_c is conduction loss from plate

A is plate area

ρ is density of free stream air

C_p is specific heat of free stream air

U_∞ is velocity of free stream air

T_p is plate surface temperature

T_∞ is temperature of free stream air

Uncertainties in experimentally determined Stanton numbers are dependent on the uncertainties in the variables used in the final data reduction expression. An expression for the uncertainty in the Stanton number (δSt) may be derived from the final data reduction expression as

$$(\delta St)^2 = \left(\frac{\partial St}{\partial w}\delta w\right)^2 + \left(\frac{\partial St}{\partial q_r}\delta q_r\right)^2 + \left(\frac{\partial St}{\partial q_c}\delta q_c\right)^2 + \left(\frac{\partial St}{\partial A}\delta A\right)^2 + \left(\frac{\partial St}{\partial \rho}\delta \rho\right)^2 + \left(\frac{\partial St}{\partial C_p}\delta C_p\right)^2 + \left(\frac{\partial St}{\partial U_\infty}\delta U_\infty\right)^2 + \left(\frac{\partial St}{\partial T_p}\delta T_p\right)^2 + \left(\frac{\partial St}{\partial T_\infty}\delta T_\infty\right)^2 \qquad \text{(II-2)}$$

Substitution of the appropriate partial derivatives and division by the Stanton number gives the final uncertainty equation as

$$\left(\frac{\delta St}{St}\right)^2 = \left(\frac{w}{w-q_c-q_r}\right)^2 \left(\frac{\delta w}{w}\right)^2 + \left(\frac{-q_c}{w-q_c-q_r}\right)^2\left(\frac{\delta q_c}{q_c}\right)^2 + \left(\frac{-q_r}{w-q_c-q_r}\right)^2\left(\frac{\delta q_r}{q_r}\right)^2$$
$$+ \left(\frac{-\delta\rho}{\rho}\right)^2 + \left(\frac{-\delta C_p}{C_p}\right)^2 + \left(\frac{-\delta A}{A}\right)^2 + \left(\frac{-\delta U_\infty}{U_\infty}\right)^2$$
$$+ \left(\frac{\delta T_\infty}{T_p - T_\infty}\right)^2 + \left(\frac{\delta T_\infty}{T_p - T_\infty}\right)^2 \qquad \text{(II-3)}$$

The uncertainty in each variable used to determine the Stanton number must be estimated before the uncertainty in the Stanton number can be estimated.

Plate Heater Power

The power supplied to each plate heater is measured by a wattmeter coupled to the Automated Data Acquisition and Control System (ADACS), which in turn is connected to a microcomputer. The total uncertainty associated with power readings made with the watt transducer and ADACS system have been determined as less than ±1.0 percent based on calibration data.

Temperature

Thermistors are used to determine the free stream air temperature, the test plate temperature and the metal support rail temperature. The free stream temperature is determined with a thermistor mounted on a probe which is inserted into the free stream. Thermistors used to determine the plate and rail temperatures are inserted into holes filled with high conductivity paste located in the bottom of the plates or the side of the metal support rails, respectively.

The uncertainty in the free stream temperature determined using the probe mounted thermistor was estimated as less than ±0.2°C.

The uncertainty in the measurement of plate surface temperatures was estimated as less than ±0.2°C. This uncertainty in the plate surface temperature was arrived at by considering the calibration uncertainty, the absolute accuracy guaranteed by the manufacturer of the quartz thermometer used as the calibration standard, uncertainty introduced by the installation of the thermistor, and small gradients in the temperature within the aluminum plates.

Conductive Losses

The effective heat transfer conductances between the test plates and metal support rails were determined experimentally. Insulation was placed over the top of the test plates, which were then heated and held at a constant temperature while the rails remained unheated. Since there was negligible radiative or convective heat loss from the covered plates, the total input power to each plate heater was equal to the conductive heat transfer rate. Input power to the plates was measured with the calibrated wattmeter and the ADACS. With the temperature of the plates and support rails and the plate heater power known, the effective heat transfer conductance for each plate was determined.

During actual data-taking runs, active heating of the metal support rails kept the rail temperature near the plate temperatures and held the conduction losses within about 0.1 watt. The contribution of a conduction loss uncertainty as large as 50% to the uncertainty in the Stanton number is negligible with active heating of the rails. Thus,

the problem of uncertainty associated with conduction losses has been effectively designed away with active heating of the steel support rails.

Area

The surface area of the plates was determined from the side dimensions of the plates. The plates were manufactured with length and width tolerances of ±0.001 in. Uncertainty in the area of the plates is the root-square sum of the percent uncertainty of the two side dimensions, which is 0.030 percent.

Radiation Power Loss

Radiation from the heated test plates primarily falls in a range from 2 to 100 microns, which is within the infrared range. Clear cast acrylic has a high absorptivity and will transmit only 2% of the incident infrared radiation. Since the test plates are enclosed by the cast acrylic sheet sidewalls and top, a gray body enclosure radiation model is used. Because clear cast acrylic has a high emissivity of about .9 and because of the magnitude of the areas involved, the general gray body enclosure model simplifies to the special case of a small object in a large cavity.

The radiative heat loss from a test plate was estimated as

$$q_r = \varepsilon \sigma A(T_p^4 - T_w^4) \qquad \text{(II-4)}$$

where

ε is the emissivity of the plate surface

σ is the Stefan-Boltzmann constant

T_w is the top and side wall temperature

A high convective heat transfer coefficient on the inside surfaces of the top and side walls will maintain the inside surface temperature of the acrylic sheet near the freestream air temperature. Thus, the temperature of the surfaces seen by the plates is assumed to be equal to the freestream air temperature and the radiation loss is estimated as

$$q_r = \varepsilon\sigma A(T_p^4 - T_\infty^4) \qquad \text{(II-5)}$$

Uncertainty in the radiation losses from the plates is dependent upon the uncertainties in the plate surface emissivity, the plate area, the temperature of the plates and the assumption of taking the enclosure wall temperature equal to the freestream temperature.

$$(\delta q_r)^2 = \left(\frac{\partial q_r}{\partial \varepsilon}\delta\varepsilon\right)^2 + \left(\frac{\partial q_r}{\partial A}\delta A\right)^2 + \left(\frac{\partial q_r}{\partial T_p}\delta T_p\right)^2 + \left(\frac{\partial q_r}{\partial T_\infty}\delta T_\infty\right)^2 \qquad \text{(II-6)}$$

Substitution of the appropriate partials into the expression above gives the final radiation loss uncertainty expression,

$$\left(\frac{\delta q_r}{q_r}\right)^2 = \left(\frac{\delta\varepsilon}{\varepsilon}\right)^2 + \left(\frac{-\delta A}{A}\right)^2 + \left(\frac{4T_p^3}{T_p^4 - T_\infty^4}\right)^2\left(\frac{\delta T_p}{T_p}\right)^2 + \left(\frac{-4T_\infty^3}{T_p^4 - T_\infty^4}\right)^2\left(\frac{\delta T_\infty}{T_\infty}\right)^2 \qquad \text{(II-7)}$$

The value of the emissivity is heavily dependent on the surface condition of the plates. Typical values of emissivity are 0.05 for a polished electroplated nickel surface at 23°C, 0.11 for an unpolished electroplated nickel surface at 20°C, and 0.37 for heavily oxidized nickel at 200°C. The emissivity of unpolished electroplated nickel with a hefty uncertainty of ±.05 was taken as the emissivity of the plates.

The minimum possible temperature of the enclosure walls would be the ambient temperature, which usually is lower than the freestream by less than 6°C. Thus, a conservative estimate of the uncertainty in taking the enclosure temperature as equal to the freestream temperature is 6°C. This seemingly large uncertainty has negligible effect on the total uncertainty in the estimated radiation loss. Thus, the total estimated uncertainty in the radiation heat loss, which is almost entirely due to uncertainty in the emissivity, is 45 percent.

Density and Specific Heat

The air in the THTTF is actually a mixture of dry air and water vapor. Therefore, fluid properties such as density and specific heat for the test air depend on the ratio of dry air and water vapor in the mixture. The ratio of dry air and water vapor is reflected by the partial pressures of each. The density and specific heat of the mixture may be expressed in terms of the partial pressures of the dry air and water vapor.

Uncertainty in the density of the test air, (±.7 percent) is mainly due to uncertainty in the relative humidity of the damp air and due to the use of ideal gas relations for non-ideal gases. Uncertainty in the effective specific heat of the mixture is also dependent on the relative humidity but is only 0.1 percent.

Velocity

A pitot probe is used to determine the freestream velocity. The pitot probe channels the stagnation pressure and static pressure exerted by the freestream into a pressure transducer so that the

difference between these two pressures can be monitored. Two calibrated pressure transducers with ranges of 0-0.08 psi and 0-0.5 psi and with calibration uncertainties of less than ±0.5 percent of reading are used for measuring the stagnation to static pressure difference.

Once the difference between the stagnation and static pressures is known, the freestream velocity may be determined from

$$U_\infty = \left(\frac{2\Delta p}{\rho}\right)^{1/2} \qquad \text{(II-8)}$$

where

U_∞ = freestream velocity

Δp = stagnation to static pressure difference

ρ = freestream density.

The uncertainty in the freestream velocity is dependent on the uncertainties in the pressure difference measured by the pressure transducer, on the uncertainty in the density, and on the uncertainty associated with the use and alignment of the pitot probe:

$$(\delta U_\infty)^2 = \left(\frac{\partial U_\infty}{\partial \Delta p}\,\delta \Delta p\right)^2 + \left(\frac{\partial U_\infty}{\partial \rho}\,\delta \rho\right)^2 + (\delta U_\infty)^2_{use} \qquad \text{(II-9)}$$

Substitution of appropriate partials and division by the velocity gives the velocity percent uncertainty expression

$$\left(\frac{\delta U_\infty}{U_\infty}\right)^2 = \left(\frac{1}{2}\right)^2\left(\frac{\delta \Delta p}{\Delta p}\right)^2 + \left(\frac{1}{2}\right)^2\left(\frac{\delta \rho}{\rho}\right)^2 + \left(\frac{\delta U_\infty}{U_\infty}\right)^2_{use} \qquad \text{(II-10)}$$

Uncertainty in the velocity due to errors caused by pitot probe use and misalignment have been estimated at 0.5 percent since the freestream flow is relatively uniform and free of pertubations and since the pitot probe is very carefully aligned with the flow. Thus, from Equation (II-10), the total uncertainty in freestream velocity is estimated as 0.8 percent.

Final Uncertainty

Uncertainties needed to evaluate the Stanton number uncertainty have been estimated as summarized in Table II-1. The resulting estimates of the uncertainties in two experimentally determined Stanton numbers are given in Table II-2. The uncertainties in the experimentally determined Stanton numbers are mainly due to uncertainties in the measurements of the plate heater power, the plate surface temperature and the free stream temperature. Uncertainties in the radiation loss, the density and the velocity are also important but usually less significant. Stanton number uncertainty contributed by uncertainties in the conduction loss, the plate area and the specific heat are negligible.

TABLE II-1

Variable Uncertainties

Variable	Uncertainty
w	±1%
q_r	±45%
q_c	±50%
A	±0.03%
ρ	±0.7%
C_p	±0.1%
U_∞	±0.7%
T_p	±0.2°C
T_∞	±0.2°C

TABLE II-2

Experimental Stanton Number Uncertainty

U_∞ m/s	Plate #	w watt	q_r watt	q_c watt	$T_p - T_\infty$ °C	St	$\delta St/St$ %
42.6	2	85.3	.54	-.06	15.1	0.00240	2.1
12.0	23	23.2	.61	.05	18.0	0.00187	2.2

END

9-87

DTIC